Journal of Applied Polymer Science

Annealing-promoted unidirectional migration of organic-modified nanoparticles embedded two-dimensionally in polymer thin films

Yang Liu,[1] Takumi Kato,[1] Masaki Kubo,[1] Ken-Ichi Sugioka,[2] Takao Tsukada,[1] Seiichi Takami,[3] Tadafumi Adschiri[4]

[1]Department of Chemical Engineering, Tohoku University, Aoba-Ku, Sendai 980-8579, Japan
[2]Department of Mechanical Systems Engineering, Toyama Prefectural University, Kurokawa, Imizu 939-0398, Japan
[3]Institute of Multidisciplinary Research for Advanced Materials, Tohoku University, Aoba-Ku, Sendai 980-8577, Japan
[4]WPI Advanced Institute for Materials Research, Tohoku University, Aoba-Ku, Sendai 980-8577, Japan
Correspondence to: M. Kubo (E-mail: kubo@pcel.che.tohoku.ac.jp)

ABSTRACT: The spatial structures of oleic acid-modified CeO_2 nanoparticles in polystyrene (PS) thin films spin-coated on silicon substrates were observed by transmission electron microscopy, when the films underwent thermal annealing above the glass-transition temperature of PS. Before annealing, the nanoparticles have segregated to the surface of the films, and formed two-dimensional spatial structures in the PS films. Then, the nanoparticles migrated away from the film surface to the substrate/film interface during thermal annealing, maintaining the two-dimensional spatial structures. In addition, we demonstrated that such unidirectional migration of nanoparticles across the PS film occurs regardless of the characteristics of the substrate surface, the concentration of nanoparticles, and the thickness of the films. © 2015 Wiley Periodicals, Inc. J. Appl. Polym. Sci. **2015**, *132*, 42760.

KEYWORDS: composites; films; microscopy; nanoparticles; nanowires and nanocrystals; polystyrene

Received 31 March 2015; accepted 22 July 2015
DOI: 10.1002/app.42760

INTRODUCTION

Thin films composed of polymers into which nanoscale inorganic particles are incorporated, namely, polymer nanocomposite thin films, have attracted much attention because their properties, such as magnetism, electric and thermal conductivities, and refractive indices, are significantly different from those of pure host polymer films. The properties of polymer nanocomposite thin films can be controlled by not only the combination of host polymers and nanoparticles of different sizes and morphologies, but also the spatial structures of nanoparticles in the polymer films. The spatial structures, which are assemblies of nanoparticles, i.e., two- or three-dimensional nanostructures, in polymer films are formed by the self-assembly of nanoparticles. Therefore, numerous applications can be expected, such as sensors,[1–3] self-healing surfaces,[4] conjugated polymer photovoltaic cells,[5–8] optical and optoelectronic devices,[9,10] and electrochemical devices,[11,12] by utilizing the properties dependent on the spatial structures of nanoparticles in polymer films. In addition, the spatial structures of nanoparticles may affect the formation of topological defects in polymer nanocomposite thin films, e.g., dewetting of the films.[13,14]

To manufacture polymer nanocomposite thin films, a solvent-casting technique is commonly used, where the thin films are deposited on solid substrates by spin- or dip-coating with solutions of an organic solvent containing polymers and nanoparticles, followed by evaporating the solvent. The polymer nanocomposite thin films may be thermally annealed or exposed to organic solvent vapors in the post processes of solvent casting. The self-assembly of nanoparticles in polymers, which is governed by the balance between entropic and enthalpic effects, determines the spatial structures of the polymer nanocomposite thin films in the above processes. In addition, the nonequilibrium processes themselves, such as shear flow, solvent evaporation, or heating during the manufacture of thin films, also affect the spatial structures of nanoparticles in polymer films. Krishnan *et al.*[13,15] demonstrated that the fine control of entropic effects enabled the manufacture of layered polymer nanocomposite thin films in which the nanoparticles segregate to the interface with the substrate upon thermal annealing, where the grafted chains are chemically the same as the host chains. However, the situation in which the grafted chains are chemically different from the host chains has not been thoroughly discussed. Therefore, it is important to understand the contributions of enthalpic and entropic effects,[16,17] and also the nonequilibrium effects, to the self-assembly of nanoparticles in polymer thin films. Moreover, the spatial assembly of nanoparticles in polymer thin films requires an understanding of nanoparticle dynamics.[18,19]

Recently, Adschiri and coworkers[20,21] have developed a new method for synthesizing organic-modified nanoparticles in single-nanometer size by supercritical hydrothermal synthesis. Such nanoparticles can be dispersed completely in organic solvents, particularly at high concentrations.[22–24] Also, it is expected that polymer nanocomposite thin films with novel characteristics and two- or three-dimensional spatial structures can be fabricated by the self-assembly of such surface-modified nanoparticles in host polymers.[25]

In this work, we found that the organic-modified nanoparticles, which have first segregated to the surface of the polystyrene (PS) film on a silicon substrate, migrated toward the substrate/film interface maintaining the two-dimensional spatial structures, when the thin film underwent thermal annealing above the glass-transition temperature of PS. Such unidirectional migration allows the nanoparticles to two-dimensionally assemble themselves at any position in the thin films. Here, oleic acid-modified CeO_2 nanoparticles prepared by supercritical hydrothermal synthesis were used. The spatial structures of the CeO_2 nanoparticles in the PS thin nanocomposite films were observed by transmission electron microscopy (TEM). In addition, the surface morphologies of the PS nanocomposite thin films were observed by atomic force microscopy (AFM) to clarify their correlation with the spatial structures of the nanoparticles in the cross-sections of the films.

EXPERIMENTAL

Materials

PS standard with a weight-average molecular weight of 50,000 g mol^{-1} (GL Sciences, Japan) was used as the host polymer matrix. The glass-transition temperature of this polymer is 377 K.[26] Toluene was used as a solvent and was purchased from Wako Pure Chemical Industries, Japan. The starting materials used to synthesize oleic acid-modified CeO_2 nanoparticles, namely, cerium hydroxide and oleic acid, were purchased from Sigma Aldrich (St. Louis, MO) and Wako Pure Chemical Industries, respectively. A silicon wafer of 23 × 23 mm^2 size (Nilaco Co., Japan) was used as a substrate, whose surface was either silanized or not silanized to investigate the effect of surface hydrophobicity. Here, the cleaned silicon wafer was dipped into a cyclohexane solution containing 0.01*M* octadecyltriethoxysilane (Shin-Etsu Chemical Co., Japan) at 333 K for silanization.

Synthesis of Oleic Acid-Modified CeO_2 Nanoparticles

Oleic acid-modified ceria (CeO_2) nanoparticles were prepared by the supercritical hydrothermal synthesis method.[20] First, 0.48 mL of oleic acid and 2.5 mL of 0.1*M* $Ce(OH)_4$ aqueous solution were poured into a pressure-resistant SUS316 reactor vessel with an inner volume of 5 mL. The supercritical hydrothermal reaction was performed at 673 K for 10 min. The synthesized CeO_2 nanoparticles whose surface was modified by oleic acid were extracted from the product mixture using cyclohexane, and then were precipitated by adding ethanol as an antisolvent. The nanoparticles were separated by centrifugation at 10,000 rpm at 288 K for 10 min, and were finally re-dispersed in toluene. Figure 1 shows a TEM image of synthesized oleic acid-modified CeO_2 nanoparticles. The shape of nanoparticles was cubes, and the average side length was approximately 6 nm.

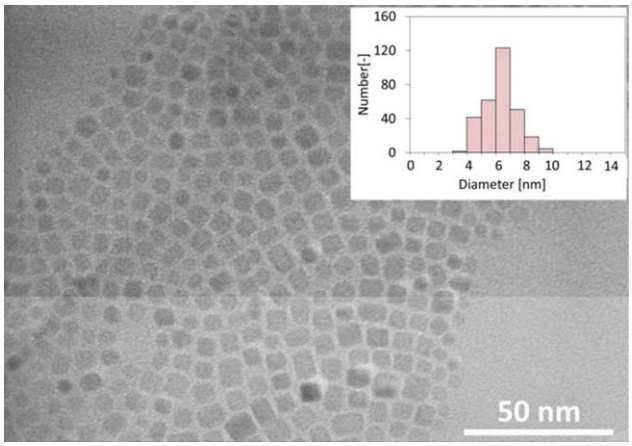

Figure 1. A TEM image of synthesized nanoparticles. Inset: histogram of nanoparticle diameter from which the average diameter was found to be approximately 6 nm. [Color figure can be viewed in the online issue, which is available at wileyonlinelibrary.com.]

Preparation of PS Nanocomposite Thin Films

The procedures for the preparation of PS nanocomposite thin films and their thermal annealing were almost the same as those in our previous study.[14] Therefore, only a summary of the procedures is provided later. Toluene solutions containing PS and nanoparticles were prepared. The concentrations of PS in the solutions were adjusted to 1.8 and 3.6 wt % for the films with thicknesses of 50 and 100 nm, respectively. The nanoparticle concentrations were 10, 20, and 30 wt % for the PS nanocomposite thin films with the thickness of 50 nm, and 15 wt % for those with the thickness of 100 nm. A 140-μL solution was spin-coated (1H-D3, Mikasa Co., Japan) at 4500 rpm for 30 s onto a silicon substrate. The prepared PS nanocomposite thin films were dried at room temperature for 24 h and then annealed in air at 433 K for up to 24 h using a handmade PID-controlled hot plate.

Characterization of PS Nanocomposite Thin Films

The thicknesses of the films before and after thermal annealing were measured by ellipsometry (DHA-XA/S3-T, Mizojiri Optical Co., Japan). The surface morphologies of the films were observed by AFM (Nanocute, SII, Japan).

The spatial structures of nanoparticles in the cross-sections of the films were observed by TEM (JEM-2100F, JEOL, Japan) at an acceleration voltage of 200 kV. Here, two pieces of substrates (area: 3 × 5 mm^2 each) were adhered together using epoxy resin (AR-R30, Nichiban Co., Japan), as shown in Figure 2, and kept at room temperature for 24 h. The above sample was polished by using an ion milling system (PIPS Model 691, Gatan, Pleasanton, CA) so that the thickness finally became less than 20 nm. In some cases, Au was sputtered on the film surface to mark the location of the film/air interface.

RESULTS AND DISCUSSION

Figure 3 shows a TEM image of the spatial structure of oleic acid-modified CeO_2 nanoparticles in the PS nanocomposite thin film that was spin-coated on a silanized silicon substrate, that is, the film before thermal annealing. Here, the film thickness was 62 nm, and

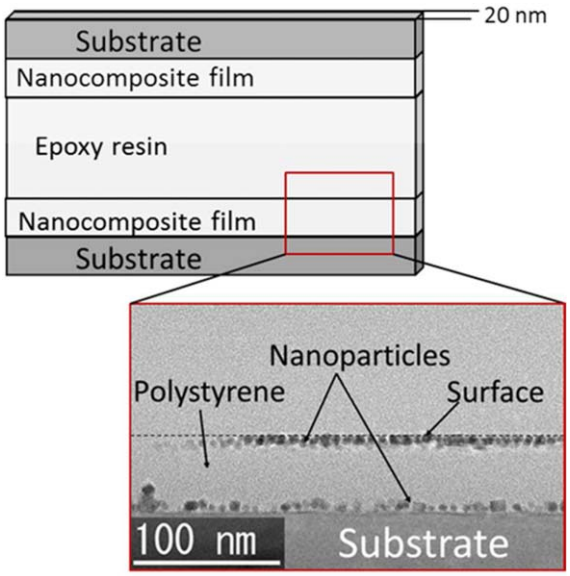

Figure 2. Schematic diagram of sample prepared for TEM observation. [Color figure can be viewed in the online issue, which is available at wileyonlinelibrary.com.]

the nanoparticle concentration in the film was 30 wt %. The dashed line in the figure denotes the location of the surface of the film, which corresponds to the film thickness measured by ellipsometry. One or two layers of nanoparticles accumulated at the film surface (film/air interface), although a few nanoparticles also existed at the substrate surface. The spatial structures of the nanoparticles in the polymer thin films were determined by the balance between entropic and enthalpic effects as mentioned earlier. According to Krishnan *et al.*,[15] the nanoparticles segregate to the substrate surface as a result of the following balance between entropic and enthalpic effects; the conformational entropy gain of the linear PS chains on moving away from the substrate is greater than the translation entropy and mixing enthalpy losses of the nanoparticles. For the system consisting of organic-modified nanoparticles and a linear PS thin film in this work, however, other enthalpic effects might play an important role in the nanoparticle assembly. Consider that the property of oleic acid on the surface of the nanoparticles is similar to that of hydrocarbons and that the surface energy of the nanoparticles is in the range from 20 to 25 mN m^{-1},[27] which is lower than that of PS (33–40.7 mN m^{-1}).[28] Then, the nanoparticles should segregate to the surface of the PS nanocomposite thin film so that the total energy of the system is minimized.

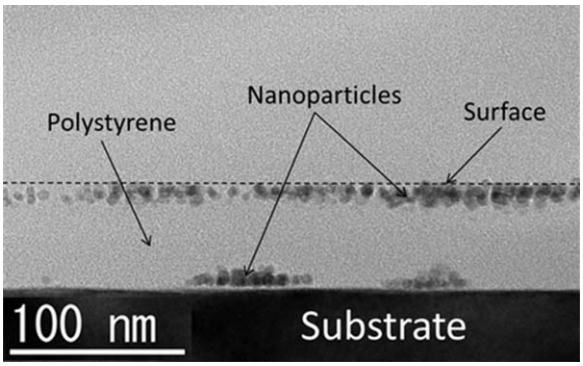

Figure 3. TEM image of cross-section of PS thin film with 30 wt % nanoparticles coated on a silanized silicon substrate before thermal annealing.

The cause of nanoparticle segregation to the PS film surface in Figure 3 was also investigated from the viewpoint of solvent evaporation during film preparation. The Peclet number, which is the ratio of convective to diffusive transport rates of nanoparticles,[29–31] is defined as:

$$Pe = \frac{6\pi\mu R_0 H\dot{E}}{kT} \quad ,$$

where, μ is the solvent viscosity, R_0 is the nanoparticle radius, H is the film thickness before evaporation starts, $\dot{E}$ is the evaporation rate, which was obtained experimentally, k is the Boltzmann constant, and T is the temperature. In this work, Pe was 0.0103, using the following values: $\mu = 1 \times 10^{-3}$ Pa s, $R_0 = 3$ nm, $H = 2.5$ μm, $\dot{E} = 0.3$ μm s^{-1}, and $T = 298$ K.

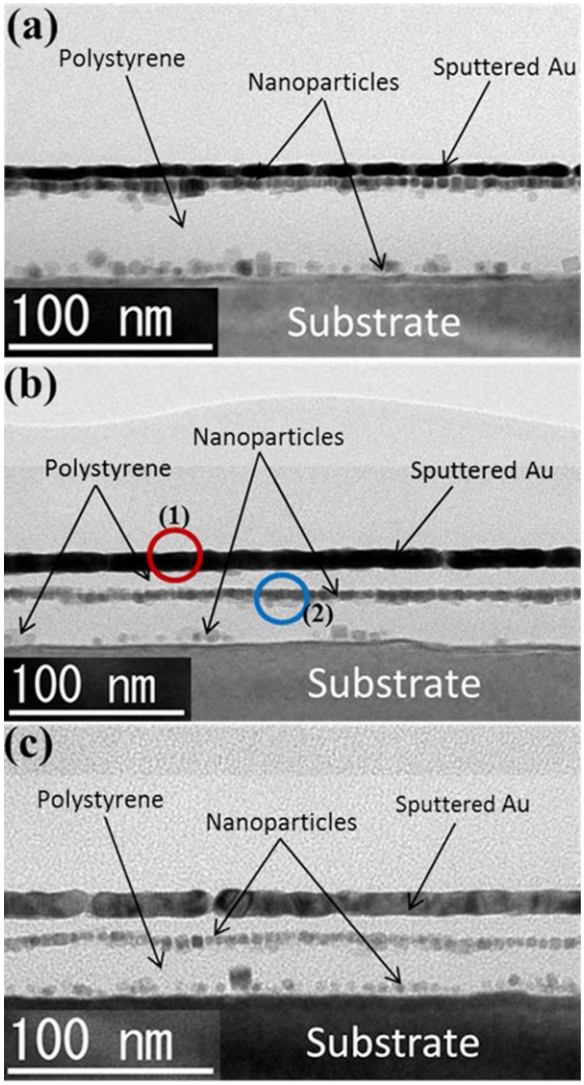

Figure 4. TEM images of films with 30 wt % nanoparticles on silanized silicon substrates. Annealing time: (a) 1 h, (b) 6 h, and (c) 24 h. [Color figure can be viewed in the online issue, which is available at wileyonlinelibrary.com.]

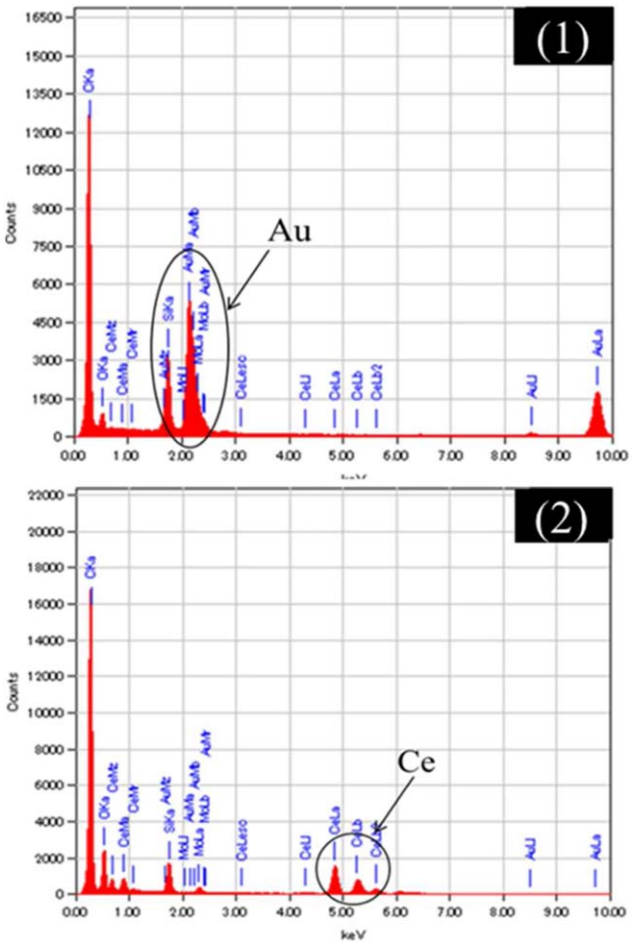

Figure 5. EDX spectra of circular regions (1) and (2) in Figure 4(b). [Color figure can be viewed in the online issue, which is available at wileyonlinelibrary.com.]

Because $Pe \ll 1$, diffusive transport of nanoparticles is dominant, namely, it was found that the nanoparticle segregation in Figure 3 is not due to evaporation-driven convective assembly.

To investigate the effect of thermal annealing on the spatial structure of the oleic acid-modified CeO_2 nanoparticles in the PS nanocomposite thin films with approximately 50 nm thickness, such as those shown in Figure 3, the films were heated to 433 K, which is much higher than the glass-transition temperature (377 K) of PS. The viscosity of PS with a molecular weight of 50,000 g mol^{-1} at 433 K was approximately 9200 Pa s, which was estimated using the experimental data reported by Plazek and O'Rourke.[32] Figure 4 shows the cross-sectional TEM images of the films with 30 wt % nanoparticles after thermal annealing for (a) 1 h, (b) 6 h, and (c) 24 h. Because it was unclear whether the location of the surface of the PS nanocomposite thin film coincided with that determined using the film thicknesses measured by ellipsometry, Au was sputtered on the surface of the film to confirm its location, and then the spatial structure of the nanoparticles in the thin film was observed by TEM. In the case of thermal annealing for 1 h, the nanoparticles still existed at the surface of the PS film. However, the nanoparticles no longer existed at the film surface after annealing for 6 h; they were embedded in the film, that is, at a distance of 37 nm from the substrate, although a few nanoparticles continued to exist at the substrate surface.

To confirm the elemental compositions in the films shown in Figure 4, energy dispersive X-ray (EDX) analysis was performed. Figure 5 shows the EDX spectra at circles (1) and (2) in Figure 4(b). The results suggest that the upper and lower layers clearly consist of Au and Ce, respectively. Figure 4(c) indicates that, after thermal annealing for 24 h, a single layer of nanoparticles was also far from the film surface and was located approximately 33 nm from the substrate. By comparing Figure 4(a,b), it was clearly demonstrated that the two-dimensionally unidirectional migration of the nanoparticles to the silicon substrate at a low speed occurred during annealing, and this migration might cease after a sufficient period.

The above results suggest that thermal annealing promotes the unidirectional migration of the nanoparticles in the PS nanocomposite thin films. However, there remains the question of whether a unidirectional migration of nanoparticles through the PS nanocomposite thin films also occurs under different conditions. To confirm it, we investigated the effects of several factors, such as the characteristics of substrate surfaces, nanoparticle concentration, and film thickness, on the spatial structures of the nanoparticles in the films.

First, the effect of octadecyl groups on the substrate surface on the spatial structure of the oleic acid-modified CeO_2 nanoparticles in the PS nanocomposite thin films with approximately 50 nm thickness was investigated, where the nanoparticle concentration was 30 wt %. We found that the nanoparticles were

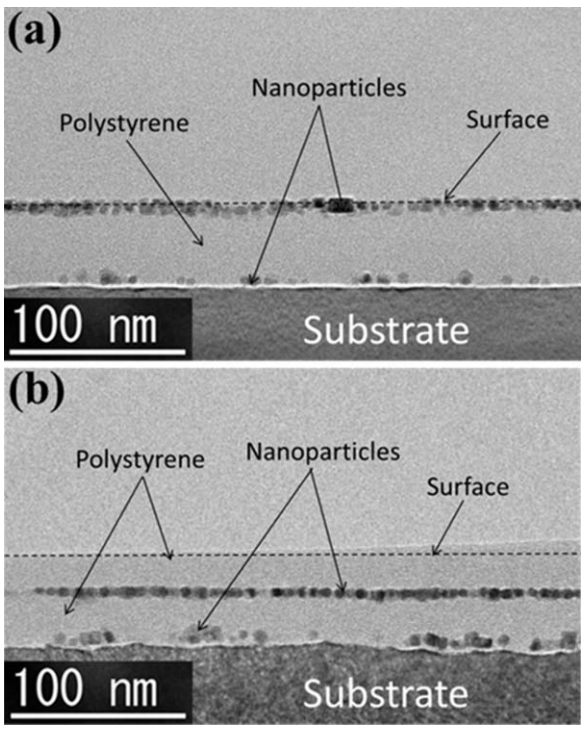

Figure 6. TEM images of films on nonsilanized silicon substrate (a) before annealing and (b) after annealing for 6 h.

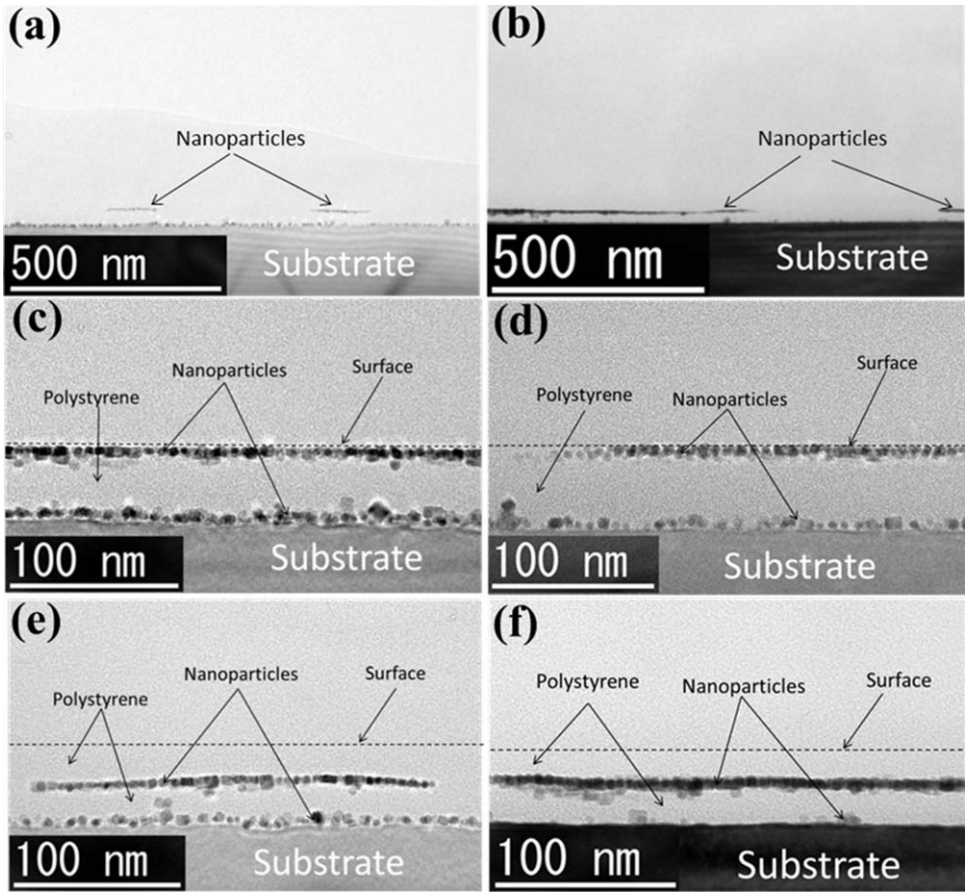

Figure 7. TEM images of films on silanized silicon substrates. (a) Nanoparticle concentration is 10 wt %, before annealing; (b) Nanoparticle concentration is 20 wt %, before annealing; (c) Magnified image of (a); (d) Magnified image of (b); (e) Nanoparticle concentration is 10 wt %, and annealing time is 6 h; (f) Nanoparticle concentration is 20 wt %, and annealing time is 6 h.

embedded at the surface of the film on a nonsilanized, bare silicon substrate before annealing [Figure 6(a)], similarly to that shown in Figure 3. The nanoparticle layer was embedded 30 nm from the substrate after annealing [Figure 6(b)]. The above results demonstrated that octadecyl groups on the substrate surface did not affect the assembly of the nanoparticles on the film surface before annealing and also their unidirectional migration in the films by thermal annealing.

To investigate the effect of nanoparticle concentration on the spatial structure of the nanoparticles in PS nanocomposite thin films, the films with approximately 50 nm thickness and different nanoparticle concentrations were annealed. Figure 7 shows the TEM images of the spatial structures of the nanoparticles in the PS nanocomposite thin films with 10 wt % [(a), (c), (e)] and 20 wt % [(b), (d), (f)] nanoparticle concentrations. Figure 7(a–d) shows the TEM images of the films before annealing, where (c) and (d) are the magnified images of (a) and (b), respectively, and Figure 7(e,f) shows the TEM images of the films after annealing for 6 h. Before annealing as shown in Figure 7(a,b), the nanoparticles discontinuously segregated at the surface of the PS nanocomposite thin films with relatively low concentrations of nanoparticles, although some nanoparticles also existed at the substrate surface. The coverage of the nanoparticles on the film surface definitely decreased with decreasing nanoparticle concentration from 30 to 10 wt %. After thermal annealing, the nanoparticles migrated from the surface of the film to the substrate surface, maintaining the two-dimensional structures of the nanoparticles, similarly to the film with 30 wt % nanoparticles.

The effect of the film thickness on the spatial structures of the nanoparticles in the PS nanocomposite thin films was also investigated. Figure 8 shows the TEM images of the spatial structures of the nanoparticles in the films with approximately 100 nm thickness. Here, the nanoparticle concentration in the film was 15 wt %, in order to adjust the surface coverage of nanoparticles on the film so that it can be the same as that on the film with 50 nm thickness and 30 wt % nanoparticle concentration. The nanoparticles segregated to the film surface before thermal annealing, whereas they were located 35 nm from the substrate after thermal annealing for 24 h, as shown in Figure 8(a,b), where Au was sputtered on the surfaces of the films to confirm their locations. These results suggest that nanoparticles in the film with 100 nm thickness also migrated far from the film surface, and that the migration distance was approximately twice as long as that with 50 nm thickness.

From the above results, it was found that the nanoparticles at the surface of the PS nanocomposite thin film migrate through the film to the substrate surface during thermal annealing, regardless of the nanoparticle concentration and film thickness. However, there

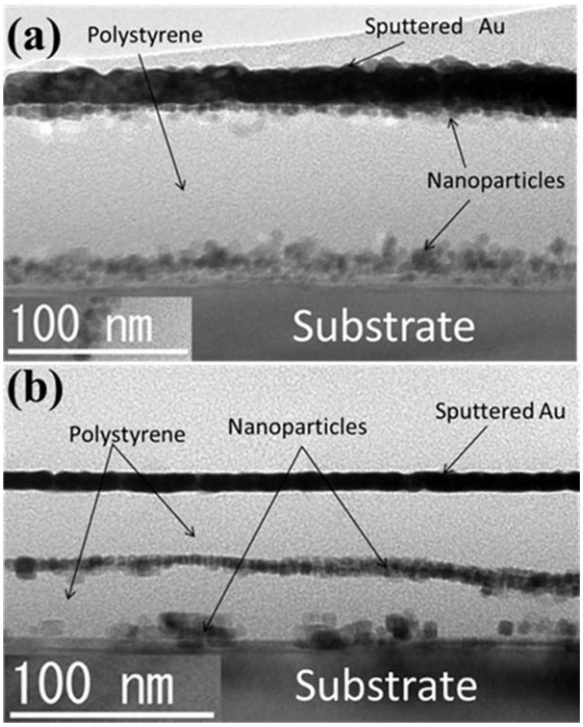

Figure 8. TEM images of films with approximately 100 nm thickness on silanized silicon substrates (a) before annealing and (b) after annealing for 24 h.

remains the question of why the nanoparticles migrated two-dimensionally through the thin film, although the nanoparticles should move randomly from the thermodynamical viewpoint.

Amarandei *et al.*[33] revealed that Au nanoparticles, whose surface energy is higher than that of PS, on the surface of PS ultrathin film with thickness of less than 30 nm were embedded in the film during thermal annealing above the glass-transition temperature of PS, similarly to oleic acid-modified CeO_2 nanoparticles in this work. They proposed a criterion for determining whether the nanoparticles are embedded in the films, being based on their free energy, which is controlled by the interaction of nanoparticles with the underlying polymer and substrate. Because the surface energy of oleic acid as a surface modifier of CeO_2 nanoparticles used in this study is lower than that of PS, it seems that the mechanism of nanoparticle embedding by Amarandei *et al.* is not applicable to the present case.

Therefore, to investigate the factors affecting the mechanism of such two-dimensionally unidirectional migration of the nanoparticles through the thin film by thermal annealing, as shown in Figures 3–8, other measurements besides TEM observation of the films have been performed. Figure 9(a) shows the time courses of film thickness during thermal annealing for four different concentrations of nanoparticles in the films with approximately 50 nm initial thickness. Here, the film thickness corresponding to each plot in the figure was individually measured by ellipsometry after thermal annealing for a given period, and then was normalized by the respective thickness before annealing. Figure 9(b) shows the effect of initial film thickness, where the nanoparticle concentrations of the films with 50 and 100 nm thicknesses were 30 and 15 wt %, respectively. The film thickness decreased sharply in the early stage of thermal annealing, and then approached gradually a constant value. Figure 9(a) also showed that increased nanoparticle concentration resulted in thinner composite films after annealing. As compared with the 100 nm thickness composite film, the 50 nm film had larger decrease in the thickness as shown in Figure 9(b). These results suggest that the thicknesses of the PS nanocomposite thin films decreased owing to the evaporation of the residual solvent, which remained in the films because the layer of nanoparticles that accumulated at the film surface, as shown in Figure 3, became highly resistant to the residual solvent transfer through the film at room temperature, which was the temperature to prepare the nanocomposite thin films before thermal annealing. The initial volume fractions of residual solvent in the films with 50 nm thickness, which were evaluated from the difference in the film thicknesses after thermal annealing for 0 and 6 h, were approximately 0.04, 0.07, and 0.17 for nanoparticle concentrations of 10, 20, and 30 wt %, respectively. The initial volume fraction in the film with 100 nm thickness was approximately 0.04 for 15 wt % nanoparticle concentration.

The effect of thermal annealing on the surface morphology of PS nanocomposite thin films was also investigated. Figure 10

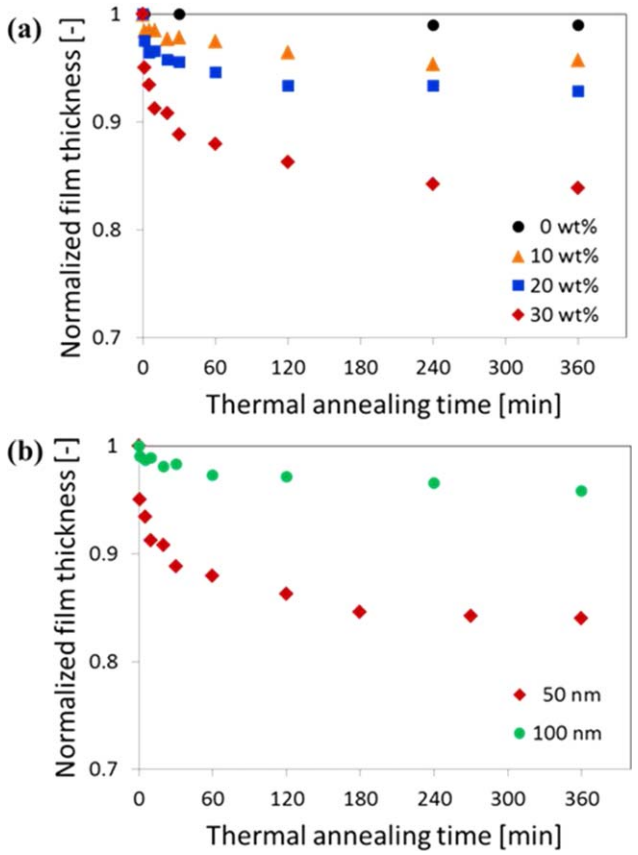

Figure 9. Time courses of film thickness during thermal annealing, where (a) nanoparticle concentration and (b) initial film thickness were varied, respectively. [Color figure can be viewed in the online issue, which is available at wileyonlinelibrary.com.]

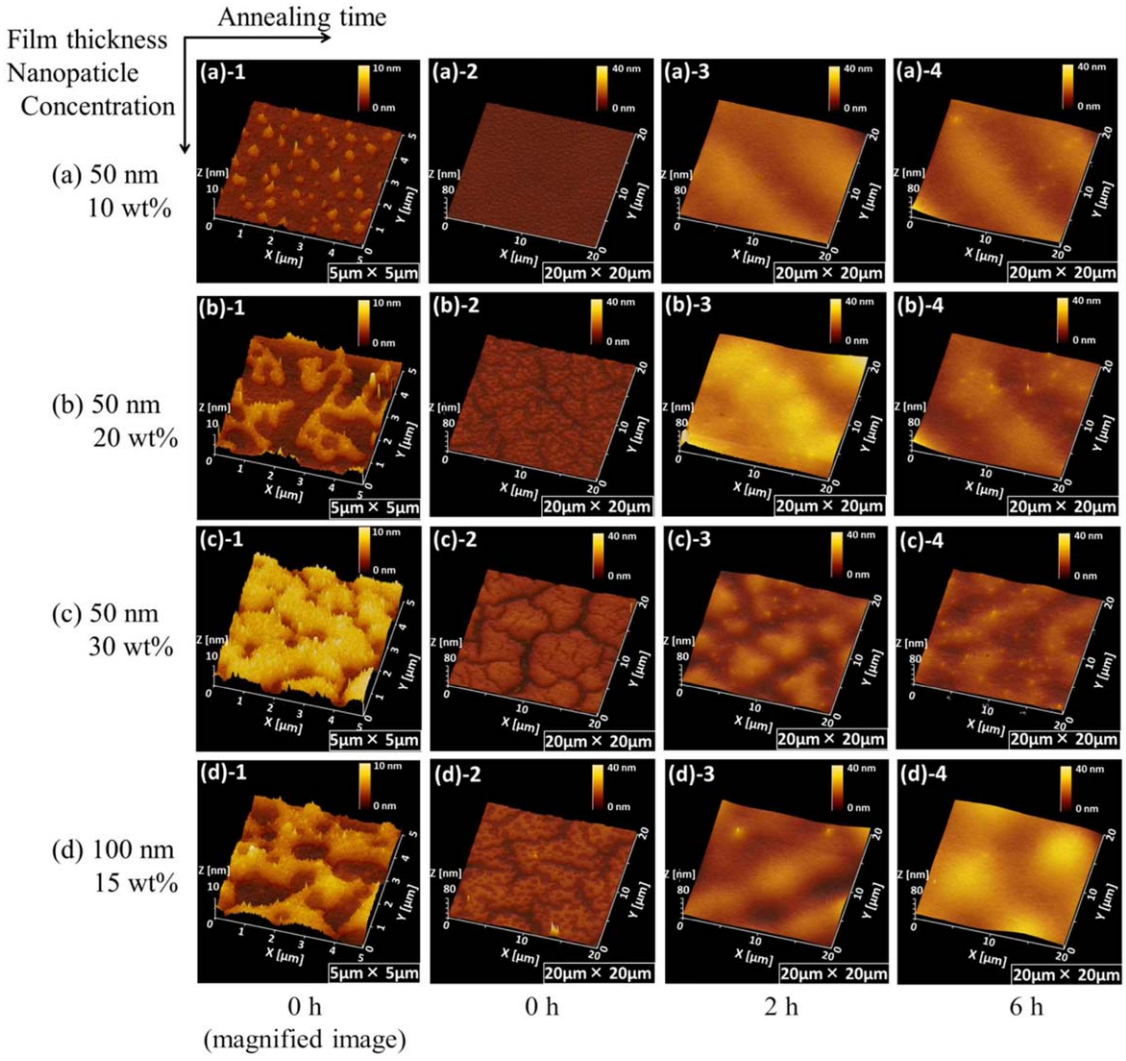

Figure 10. AFM images of films. (a) Film thickness is 50 nm, and nanoparticle concentration is 10 wt %; (b) Film thickness is 50 nm, and nanoparticle concentration is 20 wt %; (c) Film thickness is 50 nm, and nanoparticle concentration is 30 wt %; (d) Film thickness is 100 nm, and nanoparticle concentration is 15 wt %. [Color figure can be viewed in the online issue, which is available at wileyonlinelibrary.com.]

shows the AFM images of the surfaces of the PS nanocomposite thin films before thermal annealing and after thermal annealing for 2 and 6 h. Here, the images in the first column of Figure 10 are the magnified ones of the second column. The nanoparticles partially segregated to the film surface before annealing when the nanoparticle concentration was relatively low, and the surface coverage of nanoparticles on the film definitely increased as the nanoparticle concentration increased. Also, the film surfaces undulated after thermal annealing for all nanoparticle concentrations and all film thicknesses being accompanied by evaporation of residual solvents. Larger nanoparticle concentration and longer annealing resulted in the increased degree of undulation. Figure 11(a) shows the time courses of the root-mean-square roughness of PS nanocomposite thin films with approximately 50 nm initial thickness for four different nanoparticle concentrations. Figure 11(b) shows the effect of the initial film thickness, where the nanoparticle concentrations in the films with 50 and 100 nm thicknesses were 30 and 15 wt %, respectively.

It is worthwhile to note that the surface coverage of nanoparticles on the film with 100 nm thickness and 15 wt % nanoparticle concentration is smaller than that with 50 nm thickness and 30 wt % nanoparticle concentration as shown in Figure 10, because larger amount of nanoparticles segregated to the substrate before annealing for the film with 100 nm thickness as shown in Figure 8. Such a difference in the surface coverage of nanoparticles seems to be the reason why the total amount of decrease in film thickness for the film with 100 nm was smaller than that for the film with 50 nm thickness, as shown in Figure 9(b).

Comparing the TEM images in Figures 3–8 with the results in Figures 9–11, we found that the migration of nanoparticles across the PS nanocomposite thin films during thermal annealing occurred regardless of the nanoparticle concentration, although both the total amount of residual solvent in the film and the surface roughness of the film remarkably decrease as the nanoparticles concentration decrease. In other words, it seems that the residual solvent transfer through the nanocomposite thin film

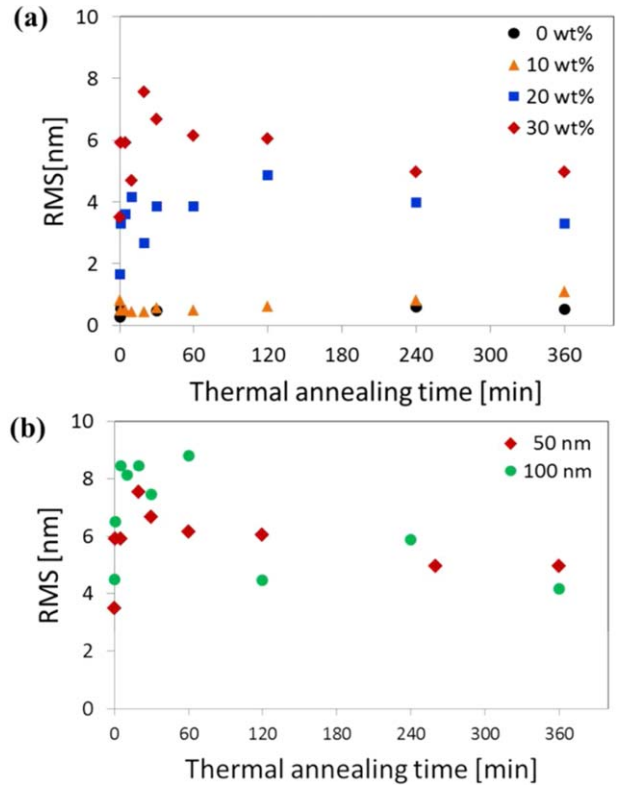

Figure 11. Time course of root-mean-square roughness of PS nanocomposite thin films for various (a) nanoparticle concentrations and (b) initial film thicknesses. [Color figure can be viewed in the online issue, which is available at wileyonlinelibrary.com.]

and the surface morphological variation of the film do not affect much the two-dimensionally unidirectional migration of the nanoparticles through the film by thermal annealing. However, the cause of such nanoparticle migration could not be understood at the present time.

CONCLUSIONS

In this work, the spatial structures of oleic-acid modified CeO_2 nanoparticles in the PS nanocomposite thin films before and after thermal annealing were investigated. Before thermal annealing, the nanoparticles segregated to the film surface. In addition, the nanoparticles migrated from the surface of PS nanocomposite thin film toward the substrate surface during thermal annealing, regardless of the nanoparticle concentration and film thickness. The hydrophobicity of the substrate did not affect the spatial structure of the nanoparticles both before and after annealing.

ACKNOWLEDGMENTS

This research was supported, in part, by Grant-in-Aid for Exploratory Research No. 26630385 from the Japan Society for the Promotion of Science (JSPS). The authors thank Dr. Takamichi Miyazaki of Tohoku University for providing technical support to take TEM images.

REFERENCES

1. Holmes, M. A.; Mackay, M. E.; Giunta, R. K. *J. Nanopart. Res.* **2007**, *9*, 753.
2. Mathew, M.; Sureshkumar, S.; Sandhyarani, N. *Colloids Surf. B* **2012**, *93*, 143.
3. Lu, S.; Luo, F.; Duan, X.; Jia, C.; Han, Y.; Huang, H. *J. Appl. Polym. Sci.* **2014**, *131*, 40634.
4. Gupta, S.; Zhang, Q.; Emrick, T.; Balazs, A. C.; Russell, T. P. *Nat. Mater.* **2006**, *5*, 229.
5. Coakley, K. M.; McGehee, M. D. *Chem. Mater.* **2004**, *16*, 4533.
6. Maier, E.; Fischereder, A.; Haas, W.; Mauthner, G.; Albering, J.; Rath, T.; Hofer, F.; List, E. J. W.; Trimmel, G. *Thin Solid Films* **2011**, *519*, 4201.
7. Hung, Y. J.; Hsu, S. S.; Wang, Y. T.; Chang, C. H.; Chen, L. Y.; Su, L. Y.; Huang, J. *J. Nanotechnology* **2011**, *22*, 485202.
8. Zhou, R.; Zheng, Y.; Qian, L.; Yang, Y.; Holloway, P. H.; Xue, J. *Nanoscale* **2012**, *4*, 3507.
9. Jeeju, P. P.; Sajimol, A. M.; Sreevalsa, V. G.; Varma, S. J.; Jayalekshmi, S. *Polym. Int.* **2011**, *60*, 1263.
10. Holder, E.; Tessler, N.; Rogach, A. L. *J. Mater. Chem.* **2008**. *18*, 1064.
11. Bhatt, A. S.; Bhat, D. K. *Polym. Bull.* **2012**, *68*, 253.
12. Bassim, N. D.; Dressick, W. J.; Fears, K. P.; Stroud, R. M.; Clark, T. D.; Petrovykh, D. Y. *J. Phys. Chem. C* **2012**, *116*, 1694.
13. Krishnan, R. S.; Mackay, M. E.; Duxbury, P. M.; Hawker, C. J.; Asokan, S.; Wong, M. S.; Goyette, R.; Thiyagarajan, P. *J. Phys.: Condens. Matter* **2007**, *19*, 356003.
14. Kubo, M.; Takahashi, Y.; Fuji, T.; Liu, Y.; Sugioka, K.; Tsukada, T.; Minami, K.; Adschiri, T. *Langmuir* **2014**, *30*, 8956.
15. Krishnan, R. S.; Mackay, M. E.; Duxbury, P. M.; Pastor, A.; Hawker, C. J.; Horn, B. V.; Asokan, S.; Wong, M. S. *Nano Lett.* **2007**, *7*, 484.
16. Tseng, T.; McGarrity, E. S.; Kiel, J. W.; Duxbury, P. M.; Mackay, M. E.; Frischknecht, A. L.; Asokan, S.; Wong, M. S. *Soft Matter* **2010**, *6*, 1533.
17. Stamm, M.; Sommer, J. *Nat. Mater.* **2007**, *6*, 260.
18. Tuteja, A.; Mackay, M. E. *Nano Lett.* **2007**, *7*, 1276.
19. Omari, R. A.; Aneese, A. M.; Grabowski, C. A.; Mukhopadhyay, A. *J. Phys. Chem. B* **2009**, *113*, 8449.
20. Zhang, J.; Ohara, S.; Umetsu, M.; Naka, T.; Hatakeyama, Y.; Adschiri, T. *Adv. Mater.* **2007**, *19*, 203.
21. Adschiri, T.; Lee, Y. W.; Goto, M.; Takami, S. *Green Chem.* **2011**, *13*, 1380.
22. Arita, T.; Yoo, J.; Adschiri, T. *J. Nanopart. Res.* **2010**, *12*, 2567.
23. Arita, T.; Yoo, J.; Adschiri, T. *J. Phys. Chem. C* **2011**, *115*, 3899.
24. Arita, T.; Yoo, J.; Ueda, Y.; Adschiri, T. *Chem. Lett.* **2012**, *41*, 1235.
25. Sahraneshin, A.; Asahina, S.; Togashi, T.; Singh, V.; Takami, S.; Hoji, D.; Arita, T.; Minami, K.; Adshiri, T. *Cryst. Growth Des.* **2012**, *12*, 5219.
26. Claudy, P.; Létoffé, J. M.; Camberlain, Y.; Pascault, J. P. *Polym. Bull.* **1983**, *9*, 208.

27. Jasper, J. J. *J. Phys. Chem. Ref. Data* **1972**, *1*, 841.
28. Wu, S. *J. Phys. Chem.* **1970**, *74*, 632.
29. Routh, A. F.; Zimmerman, W. B. *Chem. Eng. Sci.* **2004**, *59*, 2961.
30. Cardinal, C. M.; Jung, Y. D.; Ahn, K. H.; Francis, L. F. *AIChE J.* **2010**, *56*, 2769.
31. Buss, F.; Roberts, C. C.; Crawford, K. S.; Peters, K.; Francis, L. F. *J. Colloid Interface Sci.* **2011**, *359*, 112.
32. Plazek, D. J.; O'Rourke, V. M. *J. Polym. Sci.* **1971**, *9*, 209.
33. Amarandei, G.; Clancy, I.; O'Dwyer, C.; Arousian, A.; Corcoran, D. *ACS Appl. Mater. Interfaces* **2014**, *6*, 20758.